Organoids as a model to study intestinal and liver dysfunction in severe malnutrition

Horcas-Nieto, José M.; Versloot, Christian J.; Langelaar-Makkinje, Miriam; Gerding, Albert; Blokzijl, Tjasso; Koster, Mirjam H.; Baanstra, Mirjam; Martini, Ingrid A.; Coppes, Robert P.; Bourdon, Céline

Published in:
Biochimica et Biophysica Acta - Molecular Basis of Disease

DOI:
10.1016/j.bbadis.2022.166635

Publication date:
2023

BBA - Molecular Basis of Disease 1869 (2023) 166635

Contents lists available at ScienceDirect

BBA - Molecular Basis of Disease

journal homepage: www.elsevier.com/locate/bbadis

Organoids as a model to study intestinal and liver dysfunction in severe malnutrition

José M. Horcas-Nieto [a,1], Christian J. Versloot [a,1], Miriam Langelaar-Makkinje [a], Albert Gerding [a,b], Tjasso Blokzijl [c], Mirjam H. Koster [a], Mirjam Baanstra [d], Ingrid A. Martini [b], Robert P. Coppes [d], Céline Bourdon [e], Sven C.D. van Ijzendoorn [d], Peter Kim [e,h], Robert H. J. Bandsma [a,e,f,g,*,1], Barbara M. Bakker [a,**]

[a] Laboratory of Pediatrics, Center for Liver, Digestive and Metabolic Diseases, University of Groningen, University Medical Center Groningen, the Netherlands
[b] Department of Laboratory Medicine, University of Groningen, University Medical Center Groningen, Groningen, the Netherlands
[c] Department of Gastroenterology and Hepatology, University of Groningen, University Medical Center Groningen, Groningen, the Netherlands
[d] Department of Biomedical Sciences of Cell & Systems, Section Molecular Cell Biology, University of Groningen, University Medical Center Groningen, Groningen, the Netherlands
[e] Translational Medicine, Peter Gilgan Centre for Research and Learning, The Hospital for Sick Children, Toronto, ON, Canada
[f] Department of Nutritional Sciences, Faculty of Medicine, University of Toronto, Toronto, ON, Canada
[g] Division of Gastroenterology, Hepatology, and Nutrition, The Hospital for Sick Children, Toronto, ON, Canada
[h] Department of Biochemistry, University of Toronto, Toronto, ON, Canada

ARTICLE INFO

Keywords:
Malnutrition
Organoids
Amino acids
Peroxisomes
Mitochondria

ABSTRACT

Hospitalized children with severe malnutrition face high mortality rates and often suffer from hepatic and intestinal dysfunction, with negative impacts on their survival. New treatments cannot be developed without understanding the underlying pathophysiology. We have established and characterized translational organoid models of severe malnutrition of the liver and the intestine. In these models, amino acid starvation recapitulates the expected organ-specific functional changes (e.g., hepatic steatosis, barrier dysfunction) accompanied by reduced mitochondrial and peroxisomal proteins, and altered intestinal tight junction proteins. Re-supplementation of amino acids or pharmacological interventions with rapamycin or fenofibrate lead to partial recovery. Restoration of protein levels aligned with signs of improved peroxisomal function in both organoids, and increased mitochondrial proteins and tight junction protein claudin-3 in intestinal organoids. We present two organoid models as novel tools to gain mechanistic insights and to act as a testing platform for potential treatments for intestinal and hepatic dysfunction in severe malnutrition.

1. Introduction

The recent discovery of organoids has opened exciting possibilities for studying diseases, modeling cell development and applying them as therapeutic tools [1–4]. Their three dimensional and proliferative nature grants them the ability to maintain many of their organ functions, which makes them a physiologically relevant system to study diseases [5]. Organoids have been used to understand organ-specific metabolism [6,7] and to investigate the effect of nutrients on organ homeostasis [8]. Here, we present two organoid models as tools to study the impact of severe macronutrient deficiency on organ function, the role of organelle homeostasis, and study the effects of putative therapeutic compounds.

Nutritional deficiencies compromise organ function and disrupt cellular metabolism [9]. Children with severe malnutrition present with

Abbreviations: OCR, oxygen consumption rate; CBC, crypt base columnar.

* Correspondence to: R. Bandsma, Division of Gastroenterology, Hepatology and Nutrition, The Hospital for Sick Children, 555 University Avenue, M5G 1X8 Toronto, Ontario, Canada.
** Correspondence to: B. M. Bakker, Department of Pediatrics, University of Groningen, University Medical Center Groningen, Antonius Deusinglaan 1, 9713 AV Groningen, the Netherlands.
E-mail addresses: robert.bandsma@sickkids.ca (R.H.J. Bandsma), b.m.bakker01@umcg.nl (B.M. Bakker).
[1] These authors contributed equally to this work.

https://doi.org/10.1016/j.bbadis.2022.166635
Received 14 October 2022; Received in revised form 2 December 2022; Accepted 20 December 2022
Available online 26 December 2022

the most severe form of macronutrient deficiency. In developing countries, low protein diets are common, as staple foods are often high in carbohydrates and relatively low in protein (e.g. maize). This together with low food diversity and high food insecurity is thought to contribute to the development of severe malnutrition [10]. Severely malnourished children face high mortality rates when admitted to hospital for treatment of acute, mostly infectious, illnesses (e.g. 23–46 % in African hospitals) [11–14]. These children often show signs of hepatic dysfunction (e.g. hypoglycaemia, bile acid dysregulation) and intestinal dysfunction (e.g. diarrhea, increased intestinal permeability), both of which have negative impacts on their survival [15–18]. Children with severe malnutrition are extremely vulnerable and simple re-feeding protocols do not produce acceptable levels of recovery, thus the development of co-therapies are urgently needed. Clinical studies have provided some insight into the pathophysiology of the functional impairments in severe malnutrition and suggest that disrupted cellular metabolism may play a key role. Data from severely malnourished children suggests that liver fat accumulation, i.e., hepatic steatosis, is caused by impaired lipid oxidation rather than impaired secretion of lipids [19,20]. In support, post-mortem electron microscopy images revealed hepatocytes to have dysmorphic mitochondria and a decreased number of peroxisomes, which are two of the main lipid-oxidation organelles [21]. Some studies have also reported mitochondrial morphological changes in the small intestine of severely malnourished children [22–25], but their causal impact on intestinal dysfunction in severe malnutrition has not been demonstrated. Yet, a growing body of evidence suggests a pivotal role of mitochondria in maintaining intestinal homeostasis [26–28]. Further mechanistic insight is hindered by the need of invasive sampling (e.g. biopsies) in this vulnerable patient population living in low-resource settings.

To overcome these limitations, animal models have been developed and used to start unravelling the role of organelle dysfunction induced by severe malnutrition. Data from low-protein fed rodents supports the existence of a link between loss of peroxisomes, impaired mitochondrial function and the development of hepatic steatosis in severe malnutrition [29,30]. While a role of peroxisomes and mitochondria is also suspected in malnutrition-induced intestinal dysfunction, this has not yet been described. In vivo work is extremely valuable but does not offer the high-throughput capacity of in vitro models to analyse in-depth organelle dynamics and screen for potential interventions. In cultured cells, amino acid deprivation can lead to peroxisomal degradation [29] and altered mitochondrial respiration [31,32]. However, these two-dimensional cell cultures are less suitable for extrapolating to organ function. Organoids have the advantages of cell culture – ease of sampling and control of nutrient concentrations – while maintaining broader functionality of the modelled organ [33,34].

The aim of this study was to develop and characterize translational organoid models of severe malnutrition of the liver and the intestine. Amino-acid deprivation in organoids compromised both hepatic function and intestinal structure and function in a similar way as found in vivo with a low-protein diet. Functional changes were accompanied by reduced mitochondrial and peroxisomal proteins, which could mostly be restored by the re-supplementation of amino acids or pharmacological interventions with rapamycin or fenofibrate. Restoration of protein levels aligned with signs of improved fatty acid oxidation in hepatic organoids and increased tight junction protein claudin-3 in intestinal organoids. We conclude that organoid models are suitable to elucidate pathophysiological processes involved in severe malnutrition and to test novel therapeutic interventions.

2. Results

Hepatic and intestinal organoid lines were established from mouse biliary duct fragments and intestinal crypts, respectively. To mimic the effect of a low-protein diet, the organoids were cultured in a medium without any amino acids. Nevertheless, most amino acids were still detected at low levels in the medium, presumably originating from Matrigel degradation as well as from growth factors. (Supplementary Table 1).

2.1. Impact of amino acid starvation on structure and function of liver organoids

Liver progenitor organoids were matured into hepatocyte-like cells according to an established protocol [35]. Maturation was confirmed by the reduction in expression of stem cell markers and the increase in hepatocyte differentiation markers (e.g. *Albumin*, *Hnf-4α*, *Cyp1a2* and *Cyp3a11*) in organoids grown in differentiation medium compared to progenitors, as previously described in the literature [2]. Maturation of the organoids was also confirmed by increased albumin production, measured in the supernatant. Peroxisomal enzymes acyl-CoA oxidase 1 and catalase were significantly upregulated in the differentiated organoids, indicating the suitability of these organoids for the study of peroxisomes. (Supplementary Fig. 1). Deprivation of amino acids up to 96 h did not significantly affect the growth nor the morphology of mature hepatic organoids (Fig. 1a, b). In contrast, when liver progenitor organoids received the starvation medium, organoids remained smaller than control organoids (Supplementary Fig. 2). The different response to removal of amino acids reflects the lower proliferative state of mature hepatic organoids as indicated by lower gene expression levels of stem cells markers *Axin2* and *Lgr5* (Supplementary Fig. 1a). Starvation of mature hepatic organoids for 48 h substantially reduced levels of albumin released in the supernatant (Fig. 1c) and increased fat deposition as indicated by an accumulation of intracellular triglycerides as well as an increase in lipid droplets (Fig. 1d, e). Re-supplementation of amino acids after 48 h of starvation completely restored albumin production and significantly decreased lipid accumulation (Fig. 1d, e).

2.2. Impact of amino acid starvation on structure and function of small intestinal organoids

After 48 h of amino acid starvation, intestinal organoids were significantly smaller than non-starved organoids (Fig. 2a, b and Supplementary Fig. 4a). In addition, amino-acid-starved organoids displayed crypt atrophy and had substantially fewer crypts than control organoids (Fig. 2c, d and Supplementary Fig. 4b). Amino-acid deprivation upregulated the expression of markers of Paneth cells (lysozyme), goblet cells (mucin-2) and enteroendocrine cells (chromogranin A), but did not affect the expression of VIL1 (enterocytes) or stem cell and proliferation markers (Supplementary Fig. 5). FITC-dextran (4 and 10 kDa) leakage into the lumen of starved organoids was increased, as indicated by increased number of FITC-dextran positive organoids as well as higher luminal fluorescence, showing that amino-acid starvation compromised the intestinal barrier function (Fig. 3a–c, Supplementary Fig. 5). This is consistent with in vivo findings [36] and was supported by reduced levels of the tight-junction protein claudin-3 in amino-acid deprived intestinal organoids (Fig. 3d). Importantly, re-supplementation of amino acids restored organoid size, crypt number, claudin-3 protein level, and expression of mucin-2 and chromogranin A, and increased stem cell markers LGR5 and Axin2 (Fig. 2a–d, Supplementary Fig. 5). Restoration of intestinal barrier function by amino-acid re-supplementation could not be properly assessed with FITC-dextran due to the high amount of content (e.g. dead cells) in the organoids lumen after 96 h.

2.3. Amino-acid starvation reversibly reduces the levels of peroxisomal proteins in hepatic organoids

In vivo studies of rodents on a low-protein diet showed a decline of peroxisome numbers and altered mitochondrial morphology and function in the liver [29,30]. Compromised oxidation of fatty acids by peroxisomes and mitochondria explains hepatic steatosis in these studies.

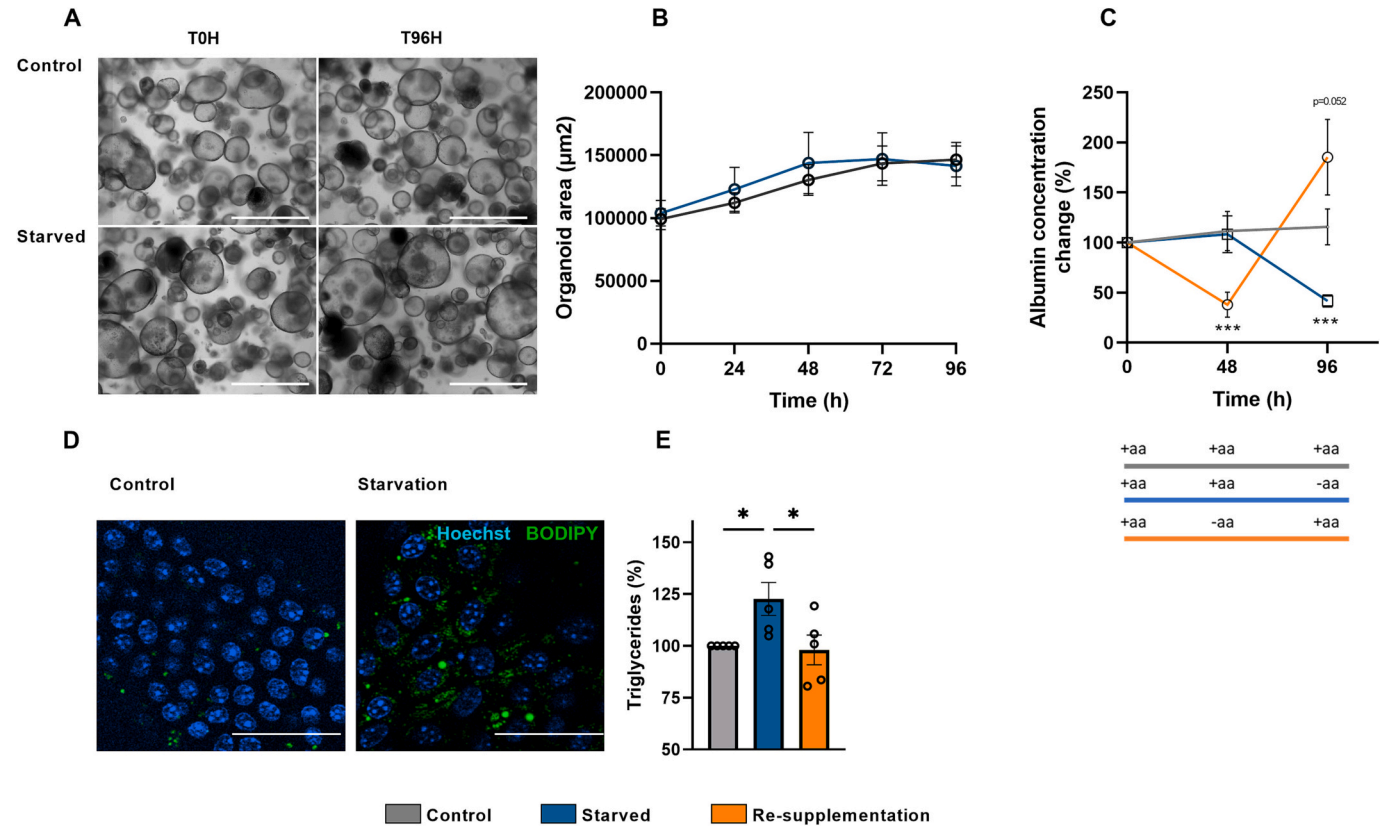

Fig. 1. Amino acid starvation of mature hepatic organoids leads to functional changes without profound morphological changes.
(A) Representative bright-field images of control and starved mature hepatic organoids prior (T0h) and after 96 h (T96h) amino acid starvation. Scale bar, 1 mm. (B) Size of organoids in complete culture medium (control, grey) or amino-acid free medium (starved, blue), expressed as size of an organoid at every time point of interest. Data based on 3 sets of independent experiments in which 25 randomly selected organoids were tracked. Error bars indicate SEM. (C) Albumin released in supernatant by organoids that were kept in complete medium throughout (control, grey), starved from 0 h to 48 h and re-supplemented with complete medium from 48 h to 96 h (re-supplementation, orange), or kept in complete medium and starved from 48 h to 96 h (starved, blue). Change in experimental conditions over time are indicated by colored bar chart. Data represents 3 biological replicates from independent experiments. Error bars indicate SEM. (*$P < 0.05$, generalised estimating equation with Tukey adjustment for post-hoc pairwise comparison). (D) Representative immunofluorescence images of control and starved mature hepatic organoids (40× magnification). BODIPY staining of fat droplets in green with Hoechst nuclei counter stain (blue). Scale bar, 50 µm. (E) Triglyceride levels in control, starved and re-supplemented organoids (as per colour legend). Data represents 5 biological replicates from independent experiments ± SEM (*$P < 0.05$, ordinary one-way ANOVA with Tukey's post hoc test).

We aimed to determine whether these findings could be recapitulated in amino-acid-deprived hepatic organoids.

Peroxisomal proliferator-activated receptor gamma coactivator 1-alpha (PGC1-α), an activator of peroxisomal and mitochondrial biogenesis [37], was reduced in the starved condition. Also, the protein levels of PMP-70, an ATP-binding cassette transporter and a major component of the peroxisomal membrane [38], was strongly reduced upon amino acid deprivation. The same was found for the peroxisomal enzymes acyl-CoA oxidase 1 (Acox-1), the first enzyme of the peroxisomal beta-oxidation and catalase, an integral part of the pathway as it scavenges the produced H_2O_2 (Fig. 4a, b). Peroxisomal fatty acid oxidation was assessed following the metabolism of phytol, a branched-chain fatty acid precursor of phytanic acid [39] (Fig. 4c). While levels of phytanic acid did not show any regulation, pristanic acid levels were significantly increased in organoids depleted of amino acids (Fig. 4d). Pristanoyl CoA is the product of the peroxisomal alpha-oxidation, which is further metabolized in the peroxisomal beta-oxidation (Fig. 4c). Phytanic acid is a branched-chain fatty acid and substrate for the peroxisomal α-oxidation, whereas pristanic acid is a substrate for β-oxidation. The increased pristanic acid levels may therefore indicate a reduction in peroxisomal beta-acid oxidation. Very-long chain fatty acids tetrasanoic and hexasanoic acids (C24 and C26, respectively) did not show any regulation (Fig. 4e), in line with the absence of long-chain fatty acids from the medium.

With respect to mitochondria, the levels of TOM-20 (a component of the 'translocase of outer membrane' (TOM) receptor complex) did not differ between control and amino acid starvation for 48 h, nor did the protein complexes of the electron transport chain (Fig. 4f, g). Total carnitine levels were unaffected after 48 h, but significantly decreased upon reintroduction of amino acids. Long-chain acyl carnitines (C14–C18) and acetyl-carnitine (C2) were decreased after 48 h of amino-acid starvation and not restored by reintroduction of amino acids (Fig. 4h).

Since in vivo studies hinted that peroxisomal loss precedes mitochondrial events [30,40], we increased the duration of the amino acid starvation to 96 h. This longer amino acid deprivation resulted in a clear reduction of mitochondrial protein markers. After 96 h of amino acid starvation, electron transport 39chain complexes I to V were significantly downregulated. TOM-20 showed a weaker downward trend ($p = 0.06$) (Fig. 5a, b). At the functional level, the longer starvation reduced ADP-stimulated respiration in the presence of palmitoyl carnitine and malate (state 3), while basal respiration remained unaffected (state 1). Uncoupled respiration (State U) showed a downward trend upon starvation, but this was not significant ($p = 0.06$). (Fig. 5c).

Re-introduction of amino acids for 48 h following 48 h of starvation recovered the PMP-70 levels to almost those of the control organoids. PGC1-α and catalase levels increased, but were not significantly different from either control or starved organoids (Fig. 4a, b). Since no

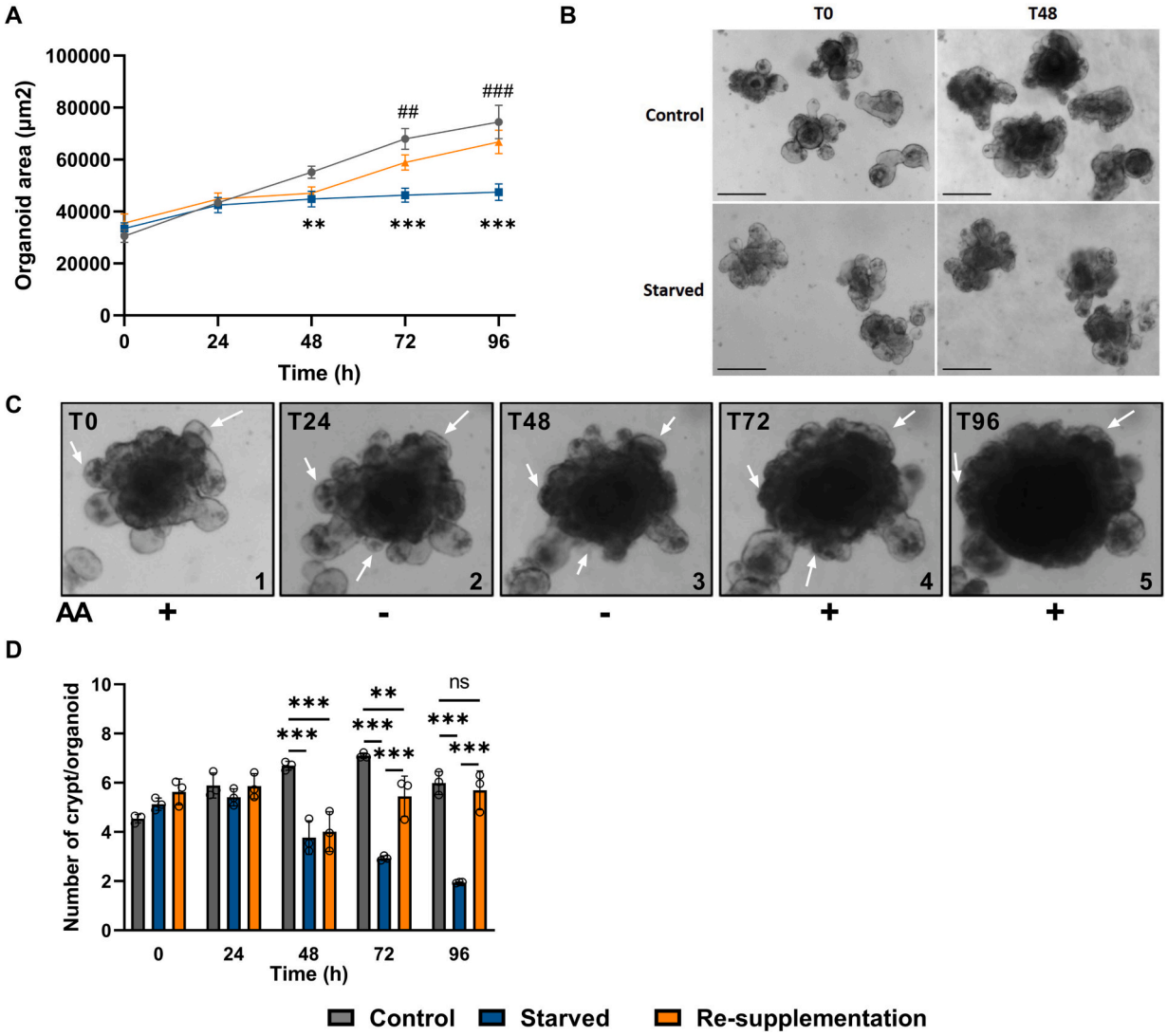

Fig. 2. Amino acid deprivation induces reversible crypt atrophy, compromised growth and barrier dysfunction in intestinal organoids.
(A) Size over time of organoids grown in complete culture medium (control, grey), amino-acid-free medium (starved, blue) or amino-acid-free medium for 48 h followed by complete culture medium for 48 h (re-supplementation, orange). Data represents the growth of 25 measured organoids in each of the 3 biological replicates from independent experiments. Error bars indicate SEM (* indicates comparison between control and starvation, # indicates comparison between starvation and re-supplementation) (***$P < 0.001$, **$P < 0.01$, *$P < 0.05$, ###$P < 0.001$, ##$P < 0.01$, #$P < 0.05$, generalised estimating equation with Tukey adjustment for post-hoc pairwise comparison). (B) Representative bright-field images of control and starved intestinal organoids at the start and after 48 h. Scale bar, 200 µm. (C) Representative bright-field images show an individual small intestinal organoid grown in complete culture medium for 3 days (C1), switched to amino acid free medium for 48 h (C2 and C3), and then placed in complete culture medium for 48 h (C4 and C5). Arrowheads indicate individual crypt domains. (D) Average number of crypts per organoid over time for control, starved and re-supplementation. Data represents the average of 25 measured organoids in each of the 3 biological replicates from three independent experiments at 5 time points. Error bars indicate SEM (**$P < 0.01$, ***$P < 0.001$, generalised estimating equation with a Poisson variance to mean relation and Tukey adjustment for post-hoc pairwise comparison.

regulation was observed in mitochondrial protein levels after 48 h, re-introduction of amino acids did not have any further effect. Due to the limited lifespan of the organoids in culture, re-supplementation after 96 h of amino acid starvation could not be done.

2.4. *Amino acid deprivation reversibly reduces mitochondrial and peroxisomal content in intestinal organoids*

In view of the key role of mitochondria and peroxisomes in intestinal homeostasis [26,41], we examined the effect of amino acid deprivation on these organelles in intestinal organoids. In contrast to hepatic organoids, amino acid starvation did not affect the protein level of PGC1-α in intestinal organoids (Fig. 6a, b). The levels of the peroxisomal proteins PMP-70 and catalase were, however, reduced in starved intestinal organoids (Fig. 6a–b).

Mitochondrial marker proteins TOM20 and Hsp60 were also down-regulated by amino acid starvation (Fig. 6a–b). Yet, the complexes of the electron transport chain were not affected by amino-acid starvation (Fig. 6a–b). Mitochondrial copy number was also significantly decreased in starvation conditions (Fig. 6d). Amino acid re-supplementation normalized all peroxisomal and mitochondrial characteristics, except the level of TOM20, which was even increased after re-supplementation (Fig. 6a–d).

2.5. *Interventions to preserve mitochondria and peroxisomes in starved organoids*

We investigated if amino-acid-deprived organoids could be used as a

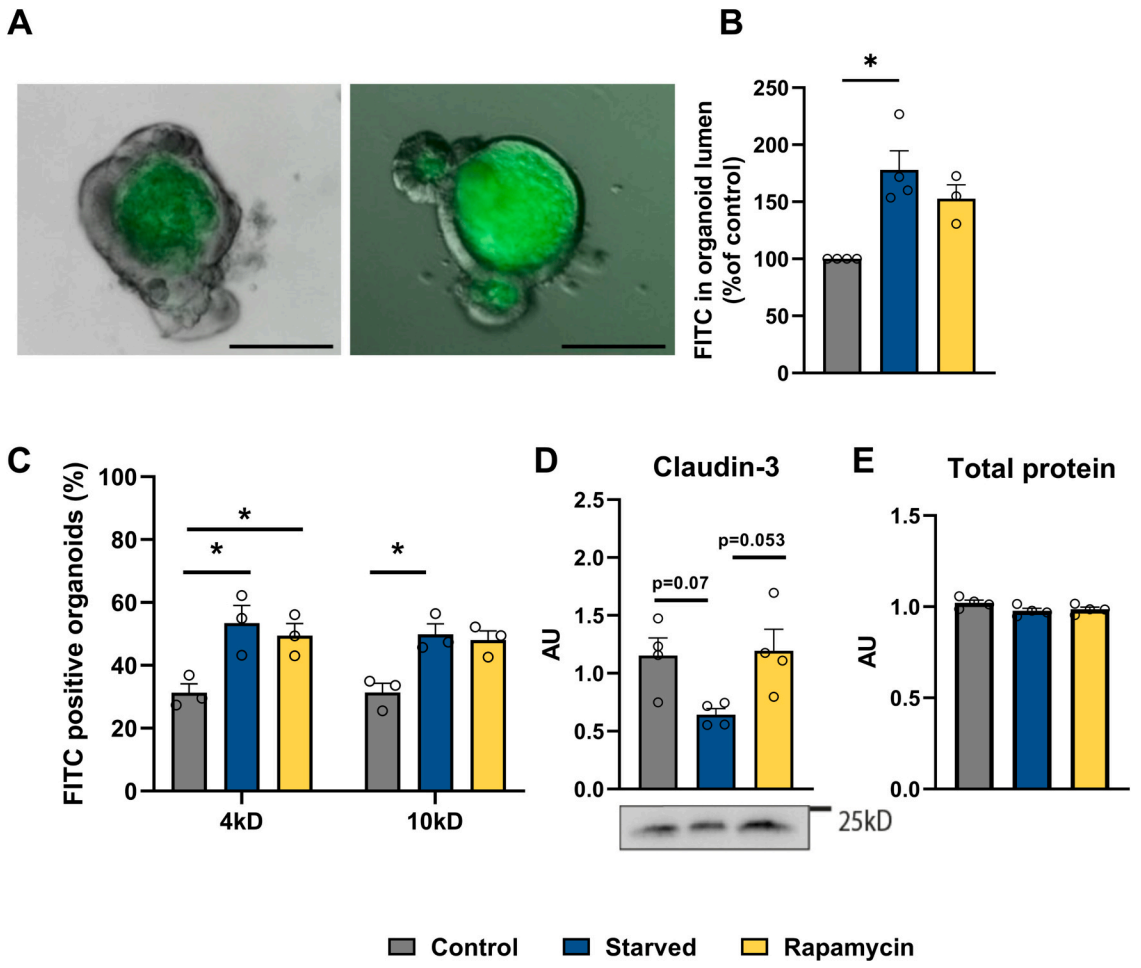

Fig. 3. Amino acid deprivation induces barrier dysfunction in intestinal organoids.
(A) Representative images for 10 kDa FITC-dextran for control (left) and starved organoid (right) (10× magnification). Scale bar, 100 μm (B) Average luminal FITC fluorescence for control, starved and rapamycin-administered organoids. Values are normalized to control organoids. Data represents mean of 3–4 biological replicates (from independent experiments) ± SEM (*$P < 0.05$, two-way ANOVA with Tukey's post hoc test). (C) Percentage of intestinal organoids with 4 or 10 kDa inside their lumen measured in organoids grown in complete culture medium (control), amino-acid-free medium (starved) and amino-acid-free medium supplemented with 2 nM rapamycin (rapamycin). Data represents mean of 3 biological replicates (from independent experiments) ± SEM (*$P < 0.05$, two-way ANOVA with Tukey's post hoc test). (D) Immunoblot quantification and representative image of tight-junction protein claudin-3 relative to total protein (see methods) for the different conditions. Normalized to total protein. Data represents mean of 3 biological replicates (from independent experiments) ± SEM. (*$P < 0.05$, **$P < 0.01$, Two-way ANOVA with Tukey's post-hoc test). (E) Relative intensity of total protein, summed over the entire lane (used for normalization to total protein, as explained in methods). Individual data points are shown for each biological replicate.

model to test pharmacological interventions to preserve organ function. As a proof of principle, we tested interventions that have already been applied in animal studies. Fenofibrate, a PPAR-α agonist, was previously shown to preserve peroxisomes and mitochondrial function in the liver of rats on a low-protein diet [30]. When administered to amino-acid starved mature hepatic organoids, fenofibrate increased levels of PGC1-α, PMP70 and catalase to values similar as the controls (Fig. 4a, b). Acox-1, the first enzyme of the peroxisomal β-oxidation was not affected by fenofibrate, nor was its substrate pristanic acid (Fig. 5a). No change was observed in the levels of mitochondrial proteins with fenofibrate treatment (Fig. 4a, b). Triglycerides were not restored upon fenofibrate treatment. Instead, addition of fenofibrate in starvation medium led to a higher accumulation of intracellular TGs (Fig. 4i).

We recently showed that rapamycin, an mTORC1 inhibitor, preserved intestinal barrier function and mitochondrial number and morphology in mice on a low protein diet (Manuscript in preparation). Likewise, in amino-acid-starved intestinal organoids, rapamycin increased the levels of mitochondrial marker protein HSP-60, although it remained lower than in control organoids (Fig. 6a, b). In addition, protein levels of PGC1-α were increased in starved rapamycin-treated organoids to a similar level as in amino-acid-re-supplemented organoids (Fig. 6a, b). Although PGC1-α is also known as an activator of peroxisomal biogenesis, rapamycin treatment did not affect the protein levels of peroxisomal proteins (Fig. 6a,b). Rapamycin treatment did preserve claudin-3 protein levels in starved organoids, suggesting preserved intestinal barrier function (Fig. 3d). However, rapamycin did not appear to decrease the FITC levels in the organoid lumen, nor the number of FITC-dextran positive organoids (Fig. 3b, c and Supplementary Fig. 6).

3. Discussion

Advances in three-dimensional cultures, in particular organoids, have opened new avenues for the development of more physiological in vitro models of organ function and diseases [1–4]. In this paper, we presented two organoid models to study pathophysiological processes and potential treatments for intestinal and hepatic dysfunction in severe malnutrition. Organ-specific manifestations of severe malnutrition were recapitulated in amino-acid-starved organoids. Concurrent mitochondrial and peroxisomal changes largely reflect in vivo findings and were

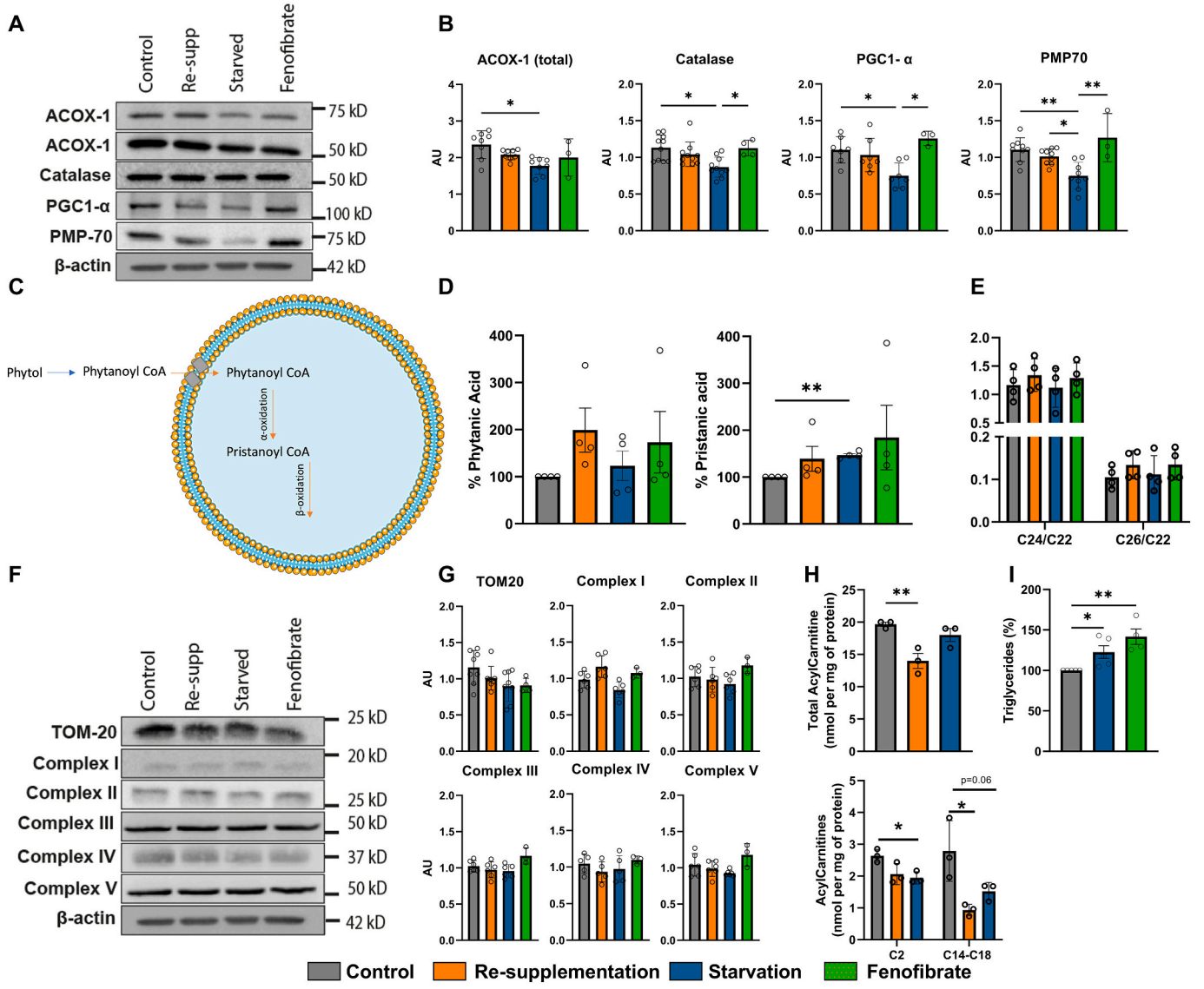

Fig. 4. Impact of amino acid starvation and re-supplementation on mitochondria and peroxisomes in mature hepatic organoids.
(A) Representative immunoblot images. (B) Peroxisomal protein levels relative to β-actin. Quantification of data shown in (A) Organoids were grown in complete culture medium throughout (control, grey), amino-acid-free medium for 48 h (starved, blue), starved from 0 h to 48 h and re-supplemented with complete medium from 48 h to 96 h (re-supplementation, orange) or in amino-acid-free medium for 48 h supplemented with 100uM fenofibrate (fenofibrate, green). Data represent mean ± SEM from 7 to 10 biological replicates and 3 biological replicates for Fenofibrate treatment (biological replicates are obtained from independent experiments) (*$P < 0.05$, **$P < 0.01$, two-way ANOVA with Tukey's post-hoc test). (C) Representative scheme of the peroxisomal pathway of phytol into phytanoyl-CoA and Pristanoyl-CoA. (D) Percentage of phytanic acid and pristanic acid in the supernatant of organoids grown in complete culture medium (control, grey), amino-acid-free medium (48 h starvation, blue), amino-acid-free medium for 48 h followed by complete culture medium for 48 h (re-supplementation, orange) or in amino-acid-free medium for 48 h supplemented with 10 μM fenofibrate (fenofibrate, green). Data represents mean of 4 biological replicates (from independent experiments) ± SEM (*$P < 0.05$, **$P < 0.01$. One-way ANOVA with Tukey's post-hoc test). (E) Ratios of very-long chain fatty acids C24/C22 and C26/C22 measured in the supernatant of organoids grown in complete culture medium (control), amino-acid-free medium (starved), amino-acid-free medium for 48 h followed by complete culture medium for 48 h (re-supplementation) or in amino-acid-free medium for 48 h supplemented with 10 μM fenofibrate Data represents mean of 4 biological replicates (from independent experiments) ± SEM (*$P < 0.05$, **$P < 0.01$. One-way ANOVA with Tukey's post-hoc test). (F) Representative immunoblot images. (G) Mitochondrial protein levels relative to β-actin. Quantification of data shown in (A) organoids were grown in complete culture medium throughout (control, grey), amino-acid-free medium for 48 h (starved, blue), starved from 0 h to 48 h and re-supplemented with complete medium from 48 h to 96 h (re-supplementation, orange) or in amino-acid-free medium for 48 h supplemented with 100uM fenofibrate (fenofibrate, green). Data represent mean ± SEM from 7 to 10 biological replicates and 3 biological replicates for Fenofibrate treatment (biological replicates are obtained from independent experiments) (*$P < 0.05$, **$P < 0.01$, two-way ANOVA with Tukey's post-hoc test). (H) Free carnitines and acylcarnitines measured in supernatant of organoids grown in complete culture medium (control), amino-acid-free medium (starved), amino-acid-free medium for 48 h followed by complete culture medium for 48 h (re-supplementation). Data represents mean of 3 biological replicates (from independent experiments) ± SEM. (*$P < 0.05$, **$P < 0.01$ Ordinary one-way ANOVA). (I) Triglyceride levels in control, starved and fenofibrate treated organoids (as per colour legend). Data represents 4–5 biological replicates from independent experiments ± SEM (*$P < 0.05$, ordinary one-way ANOVA with Tukey's post hoc test).

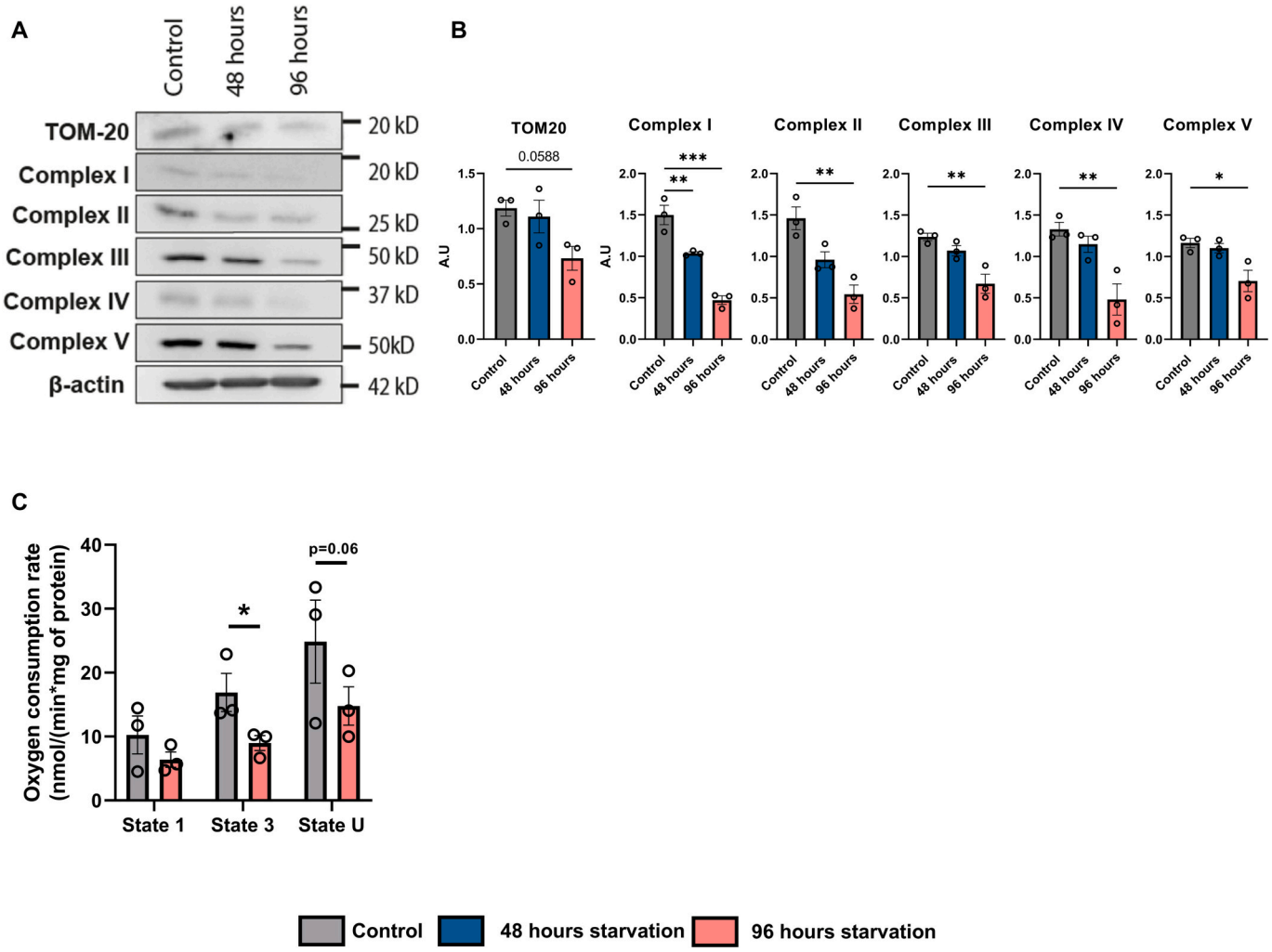

Fig. 5. Mitochondrial dysfunction after prolonged amino acid starvation in mature hepatic organoids.
Mature hepatic organoids were grown in complete culture medium throughout (control, grey), amino-acid-free medium for 48 h (48 h starvation, blue) and starved for 96 h (96 h starvation, pink). (A) Representative immunoblot images. (B) Protein levels relative to β-actin. Quantification of data shown in (A) Data represent mean ± SEM from 3 biological replicates (biological replicates are obtained from independent experiments) (*$P < 0.05$, **$P < 0.01$, one-way ANOVA with Tukey's post-hoc test). (C) Oxygen consumption rate in mature hepatic organoids measured as basal respiration (State 1) (ADP), State 3 (stimulated with palmitoyl carnitine and malate and ADP) and uncoupled respiration (State U). Data represents the mean of 3 biological replicates (from independent experiments) ± SEM. (*$P < 0.05$, **$P < 0.01$ paired *t*-test).

found to be organ-specific. We showed that amino-acid-starved organoids cannot only be used to gain mechanistic insights, but also to test pharmacological interventions.

3.1. *Functional impact of amino acid starvation on hepatic and intestinal organoids*

Mature hepatic organoids showed no morphological or size changes upon amino-acid starvation. This could be attributed to their low proliferative state, as indicated by lower stemness markers than in hepatic progenitor organoids. Their functionality was, however, substantially impaired. Albumin production dropped upon starvation, which was expected as albumin synthesis requires amino acids as precursors and is stimulated by dietary amino acids [42]. The same was observed in low-protein fed rats [30] and severely malnourished children [43]. Enlarged fat droplets, increased levels of triglycerides and elevated levels of pristanic acid point to lipid accumulation in starved hepatic organoids. Hepatic steatosis has also been commonly observed in severely malnourished children [44] and rodents on a low-protein diet [30,45]. We did not study glucose production, even though impaired hepatic glucose production reported in severely malnourished children increases the risk of hypoglycaemia and death [15,17]. The reason is that functional glucose production has rarely been studied in organoids, since the level of the essential enzyme glucose 6-phosphatase (G6PC) is typically low in vitro [46,47]. It was recently shown that organoids derived from primary hepatocytes have a higher G6PC expression [33] than organoids derived from cholangiocytes, and a normalized glycogen storage [48]. This provides a perspective to study functional glucose production in organoids.

Intestinal organoids starved for amino acids were smaller than those in complete medium, with fewer crypts and atrophy of cryptlike domains. This could point to suppressed enterocyte proliferation, as has also been shown in intestinal organoids deprived of glutamine, methionine or valine [49,50]. In starved organoids gene expression of stem cell and proliferation markers was not significantly reduced, but it was nevertheless increased upon re-supplementation. This is in line with the observed re-growth of crypts. Restoration of growth and new crypt formation after amino acid re-supplementation indicates that intestinal stem cells have the capacity to recover from prolonged amino-acid starvation. Re-growth of crypts may be attributed to rapidly cycling

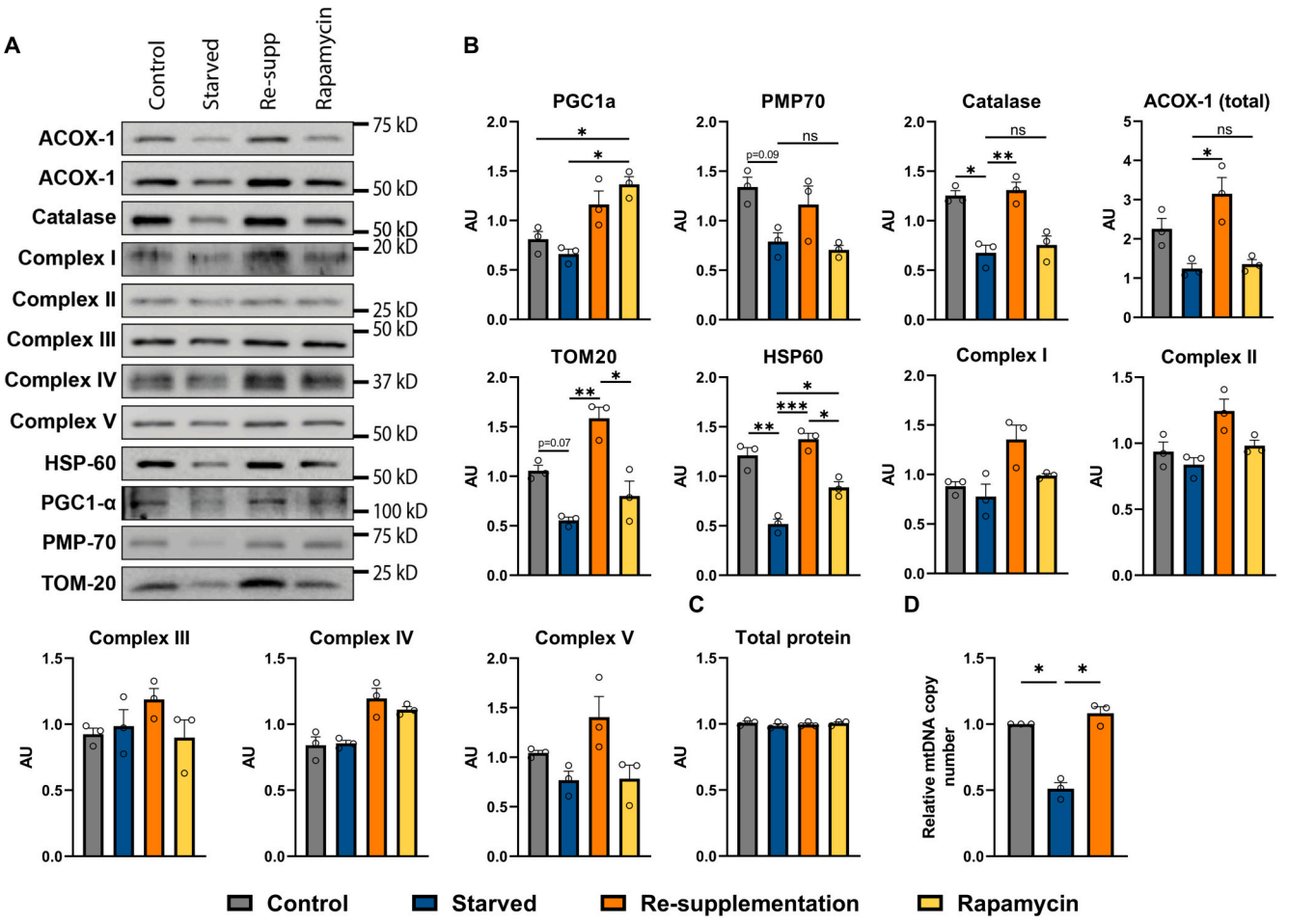

Fig. 6. Impact of amino acid starvation, re-supplementation and rapamycin on mitochondria and peroxisomes in intestinal organoids. (A) Representative immunoblot images. (B) Quantification of data shown in (A). Protein levels were normalized to total protein (see methods section). Organoids were grown in complete culture medium (control), amino-acid-free medium (starved), amino-acid-free medium for 48 h followed by complete culture medium for 48 h (re-supplementation) or in amino-acid-free medium for 48 h supplemented with 2 nM rapamycin. Data represents mean of 3 biological replicates (from independent experiments) ± SEM (*$P < 0.05$, **$P < 0.01$, ***$P < 0.001$, Two-way ANOVA with Tukey's post-hoc test). (C) Relative intensity of total protein measured in each entire lane (used for total protein normalization as explained in methods). Individual data points are shown for each biological replicate. (D) Mitochondrial copy number expressed mitochondrial DNA normalized to β-globulin as reference. Data represents mean of 3 biological replicates (from independent experiments) ± SEM. (*$P < 0.05$, **$P < 0.01$ ordinary one-way ANOVA).

Lgr5^{+} crypt base columnar (CBC) cells, which were previously found resilient to glutamine starvation [49]. Another possibility is the mobilization of another stem cell population referred to as quiescent 'reserve' stem cells (+4 position) that are activated upon injury to restore tissue homeostasis [51]. Moreover, de-differentiation of progenitor cells [52,53] as well as differentiated epithelial cells can contribute to repopulation of the stem cell niche [54,55]. Yet, the impact of prolonged amino-acid deprivation on intestinal stem cells and on de-differentiation has not been studied. Finally, the barrier dysfunction and reduction of claudin-3 in starved intestinal organoids was in agreement with reported findings in severely malnourished children [56–58] and in low-protein fed rodents [36].

3.2. *Impact of amino acid starvation on organelle homeostasis in hepatic and intestinal organoids*

We found that amino-acid starvation impacted peroxisomes earlier than mitochondria in hepatic organoids, whereas both peroxisomes and mitochondria were affected in intestinal organoids after 48 h. The disparate impact on mitochondria plausibly reflects metabolic differences between the intestine and the liver. In the liver, mitochondria are important for fatty acid oxidation, whereas in the intestine mitochondria are essential for proper stem cell function and thereby epithelial turnover [27,59]. In addition, nutrient requirements may be higher in the intestine due to the high turnover rate, which could lead to more severe mitochondrial changes when exposed to a similar nutritional insult.

In starved hepatic organoids we found that peroxisomal marker proteins were significantly decreased, which corresponded to reduced peroxisomal numbers in the liver of low-protein fed rodents [29,30]. It has been shown that peroxisomes are selectively degraded upon amino acid starvation [60,61]. Reduction of peroxisomal proteins, and particularly of Acox-1, is in line with the observed accumulation of pristanic acid in the starved organoids. Mitochondrial marker proteins and mitochondrial oxygen consumption were unaffected in 48 h starved hepatic organoids, which was very similar in rats that were fed a low-protein diet for 1 week [30]. However, after 4 weeks mitochondria had an aberrant structure and compromised fatty-acid β-oxidation in these animals, which together with a decline in peroxisomal number was thought to contribute to the observed hepatic steatosis [30]. Since it has been suggested that peroxisomal decline precedes mitochondrial decline [30], we decided to increase the starvation time in the organoids up to 96 h. This delayed onset of a mitochondrial phenotype was reproduced in the organoids: after 96 h of amino-acid starvation mitochondrial protein markers as well as functional state 3 respiration were

significantly reduced. These results are consistent with findings that defects in peroxisomal biogenesis may cause mitochondrial decline [40,62]. The decrease of acyl carnitines (already after 48 h) preceding the reduction in oxygen consumption could be explained by the system relying on fatty acids to obtain energy after removal of amino acids.

In starved intestinal organoids both mitochondrial membrane and matrix markers were lower, reminiscent of reduced mitochondrial numbers in the intestine of mice on a low-protein diet (manuscript in preparation). The decline of peroxisomal marker proteins in intestinal organoids is a novel finding for the intestine. As mitochondria play an important role in maintaining the stem cell niche [27,59], reduction in mitochondrial markers proteins could contribute to the observed crypt atrophy in the organoids. Although peroxisomes are highly abundant in the small intestine [63], little is known about the functional significance of these organelles in this organ. In Drosophila, peroxisomes are required for homeostasis of intestinal epithelium [64]. More recently, Du et al. reported that elevated peroxisome numbers are required for stem cell differentiation and epithelial repair in human, mouse and drosophila intestine [41]. Reduced or dysfunctional peroxisomes could result in epithelial instability [64] via redox stress, and compromise epithelial turnover [41]. Intestinal organoids are a versatile model to further explore the reduction of peroxisomes upon amino-acid starvation and its consequences for intestinal homeostasis.

3.3. Translation into potential treatments for severely malnourished children

We tested if targeting mitochondria and peroxisomes could preserve organ homeostasis under amino- acid deprived conditions. In starved hepatic organoids, addition of PPAR-α agonist fenofibrate partially recovered the protein expression levels of peroxisomal markers but showed no effect on pristanic acid metabolism. Fenofibrate did not recover intracellular triglyceride levels when administered during amino acid starvation. In contrast, fenofibrate treatment in low-protein fed rats significantly improved mitochondrial β-oxidation capacity resulting in reduced hepatic fat deposition [30]. In general, contrasting effects of fenofibrate on triglycerides have been described. For instance, in healthy mice fenofibrate reduced levels of triglycerides in serum but increased triglycerides in the liver. This increase in triglycerides upon fenofibrate administration has been reported to be mediated by the activation of SREBP1-c, which then activates lipogenesis [65]. These results have also been confirmed in HEPG2 cells [65]. The positive effect on peroxisomal protein levels, however, offers therapeutic potential [44]. Fenofibrate is usually well-tolerated during treatment of dyslipidemia, but side effects such as rhabdomyolysis are a risk in severely malnourished children [66]. Further investigation is required into the mechanisms of action, into the later effects of malnutrition on the mitochondria, and into the possibilities of other, possibly more specific PPAR-α-modulating dietary components (e.g. polysaturated fatty acids, flavonoids) in improving hepatic function in severe malnutrition [67,68].

In starved intestinal organoids, rapamycin treatment preserved mitochondria and peroxisomes. This coincided with higher levels of the tight junction protein claudin-3 than in starved, untreated organoids, suggesting better maintained barrier function. This preservation of claudin-3 did not translate into a protective effect at the level of permeability, which could be due to other tight junction proteins that might have been affected by amino acid deprivation. Accumulating data suggests a key role for mitochondria in maintaining the intestinal barrier [26], but for peroxisomes this is less known. Improved mitochondrial health may be attributed to stimulated mitochondrial biogenesis, as PGC1-α protein levels were increased in rapamycin-administered starved organoids. In addition, rapamycin could improve mitochondrial homeostasis via clearance of dysfunctional mitochondria through autophagy activation [69], thereby contributing to the potentially improved barrier function. The potential positive impact of rapamycin on the intestinal barrier has therapeutic implications for severely malnourished children, because it could have potential to prevent bacterial translocation-induced clinical deterioration and death [56–58].

A limitation of this study is that no human organoids were included. The choice for mouse organoids enabled us to make a direct comparison between organoids and mouse liver or intestine, particularly concerning the mitochondrial and peroxisomal phenotype. This comparison could not be made with human tissue, since invasive samples in malnourished children are scarce. A next step should be the translation to human organoids.

4. Conclusions

The results of this study support the notion that hepatic and intestinal organoid models can be used to further investigate underlying mechanisms of organ dysfunction in severe malnutrition. These models are also suitable to explore therapeutic interventions.

5. Methods

5.1. Isolation of intestinal crypts and biliary duct fragments and organoid culture

The use of crypts from the small intestine and ductal fragments from the liver of male C57BL/6 J mice between 3 and 5 weeks of age (Jackson Laboratory, Bar Harbor, ME, USA) was approved by the Central Authority for Scientific Procedures on Animals (CCD) of the Netherlands and from the University of Groningen Ethical Committee for Animal Experiments (Animal Use Protocol Number: 171504-01-001/3).

The small intestine was dissected and divided in three sections: from proximal to distal, the duodenum, jejunum and ileum. Jejunum was used to generate organoids according to a previously described protocol [1]. Intestinal organoids were kept in complete culture medium consisting of AdvDMEM/F12 plus 10 mM HEPES, 1× GlutaMax and 1 % Penicillin-Streptomycin (all Gibco), 1× N-2 Supplement (Invitrogen, CA, USA), 1× B-27 Supplement (Invitrogen), 1.25 mM N-Acetylcysteine (Sigma Aldrich, MO, USA), 10 % RSpondin Conditioned Medium (provided by Calvin J. Kuo), 50 ng/ml EGF (Peprotech, NJ, USA) and 100 ng/ml Noggin (Peprotech). Medium was changed every 2–3 days. Intestinal organoids were passaged every 5–7 days.

Ductal fragments from livers were isolated following the protocol by Broutier et al [35]. Biliary duct fragments were kept in culture expansion medium consisting of Advanced DMEM/F12 supplemented with 10 mM HEPES, 1× GlutaMax, 1 % Penicillin-Streptomycin, 1× N-2 Supplement, 1× B-27 Supplement, 10 mM Nicotinamide (Sigma Aldrich), 1.25 mM N-Acetylcysteine, 10 % RSpondin Conditioned Medium, 30 % Wnt3a CM (provided by Hans Clevers), 100 ng/ml Noggin, 50 ng/ml HGF (Peprotech), 100 ng/ml FGF-10 (Peprotech), 50 ng/ml EGF, 10 nM Leu-gastrin (Sigma Aldrich). Three days after the isolation Noggin and Wnt3a CM were removed from the medium. The medium was changed every 2–3 days. Liver organoids were passaged every 6–7 days. Expansion medium promotes the proliferation of liver stem cells as well as cholangiocytes. After three days in expansion medium, organoids were transferred to hepatocyte-differentiation medium which consisted of Advanced DMEM/F12 supplemented with 10 mM HEPES, 1× GlutaMax, 1 % Penicillin-Streptomycin, 1× N-2 Supplement, 1× B-27 Supplement, 1 mM N-Acetylcysteine, 100 ng/ml FGF-10, 50 ng/ml EGF, 10 nM Leu-gastrin, 50 nM A-83-01 (Tocris, Bristol, UK) and 10uM DAPT (Sigma Aldrich). After day 13, 3 μM dexamethasone (Sigma Aldrich) was added into the medium. Organoids were kept in differentiation medium until day 16.

5.2. Malnutrition in organoids using amino acid starvation and amino acid re-supplementation studies

To mimic malnutrition in organoids, a custom-made amino acid free

Advanced DMEM/F12 was used (Invitrogen). Apart from this amino acid free DMEM, the formulation of the culture media was identical as described above for the respective organs.

Intestinal organoids were grown in complete culture medium for three days after passage before being placed in low amino acid culture medium for 48 h. For the amino acid re-supplementation studies, organoids were placed in complete medium for further 48 h after the starvation. All organoids conditions were collected at the end of day 7.

Liver progenitor organoids were grown in complete expansion medium for 3 days after passage before being placed in differentiation medium until day 12. From day 12 to day 14 they were grown in amino acid-free medium. At the end of day 14 the organoids were placed back in complete differentiation medium until the end of day 16. For simple amino acid starvation, the organoids were starved from day 14 to day 16. All the organoids conditions were collected at the end of day 16.

5.3. Therapeutic interventions

Intestinal organoids were grown in complete culture medium until three days after the passage, then placed in amino acid-free medium for 48 h that was supplemented with rapamycin (Sigma Aldrich, MO, USA) at a final concentration of 2nM [70–72].

Hepatic organoids were grown in complete differentiation medium until day 14. From day 14 to day 16 they were grown in amino acid-free medium supplemented with fenofibrate (Sigma Aldrich) at a final concentration of either 10 or 100 μM [65], as indicated.

5.4. Amino acid measurements

Amino acid profiles were measured by GC/MS (Agilent 9575C series GC/MSD, Agilent Technologies, Amstelveen, The Netherlands) as previously described [73].

5.5. Albumin measurement

Supernatant from the hepatic organoid cultures was collected every 24 h starting from day 12 of the differentiation until day 16 and was stored at −20 °C. The concentration of albumin in the supernatant was measured using the mouse albumin ELISA kit (Abcam, Cambridge, UK) according to the manufacturer's instructions in the Synergy H4 Hybrid Microplate Reader (BioTek Instruments Inc., VT, USA).

5.6. RNA isolation, reverse transcription and quantitative real-time qPCR

Total RNA was extracted from organoids using the commercially available RNeasy Mini Kit (Qiagen, Hilden, Germany) according to the manufacturer's instructions. RNA quality and quantity was determined with NanoDrop (NanoDrop Technologies, Wilmington, DE, USA). Reverse transcription was completed with the M-MLV Reverse Transcriptase (200 U/μl) (Invitrogen) according to the manufacturer's instructions. qPCR reactions were performed using FastStart Universal SYBR Green Master (Rox) (Sigma Aldrich) in 384 well format in duplicate with 20 ng total cDNA per well in a QuantStudio 7 Flex (Thermo Fisher Scientific). All primers sequences (Integrated DNA technologies Inc., Coralville, IA, USA) are listed in Supplementary Table 2. Peptidylprolyl isomerase A (cycophilin A)(PPIA) served as endogenous control, as expression was stable between experimental groups and was used for normalization. Relative expression was calculated using the ΔΔC(t) method relative to the control organoids.

5.7. Triglyceride measurement

Organoids were collected in 1× TBS in MiliQ water. Fat was extracted using chloroform-methanol in a 2:1 ratio. Quantitative determination of hepatic triglycerides was done with the DiaSys Triglyceride FS kit (Holzheim, Germany, Cat #157109910971). Results were normalized to protein content.

5.8. BODIPY staining

Hepatic organoids were fixed in 4 % PFA for 1 h at 37 °C. Permeabilization and staining were done simultaneously in CLMS buffer (PBS, 3 % BSA, 10 mM glycine) containing 0.1 % saponine, 15 μM BODIPY (Thermo Fisher Scientific) and 5 μM Hoechst (Thermo Fisher Scientific) for 1 h at room temperature. The organoids were washed with PBS and images were acquired with an AxioObserver Z1 compound microscope, 40× objective and AxioCam Mrm3 CCD camera.

5.9. Permeability measurement (FITC)

Permeability of intestinal organoids was assessed using fluorescence markers. Organoids were incubated with FITC-dextran 4 kDa or 10 kDa (TdB Consultancy, Uppsala, Sweden) at a final concentration of 1.25 μM in their respective Ad.DMEM/F12 for 30 min at room temperature. Organoids were washed 5–10 times with PBS to remove non-specific binding. The degree of accumulation in the lumen of 15 organoids chosen at random served as a measure for permeability. Organoids were imaged with an AxioObserver Z1 compound microscope, 2.5× or 10× objective and AxioCam MRm3 CCD camera. ZEN 3.1 blue was used to measure the fluorescence in the organoid lumen. To correct for differences in background fluorescence, the intensity was measured in three different areas around the organoid. The mean intensity measured in three squares around the organoid was subtracted from the luminal fluorescence.

5.10. Immunoblotting

For Western blotting, the protocol was based on a previously published paper [74]. Organoids were collected using the respective cold Advanced DMEM/F12 (with or w/o amino acids) and kept on ice for 10 min to ensure Matrigel dissolvement. Organoids were centrifuged at 200–290*g* for 5 min followed by one wash with cold PBS. Organoids were again centrifuged and resuspended in 200uL of radio immunoprecipitation assay buffer (1%IGEPAL CA-630, 0.1 % SDS, and 0.5 % sodium deoxycholate in PBS) supplemented with Complete Protease Inhibitor Cocktail (Cat. No. 1186145001; Sigma-Aldrich), Phosphatase Inhibitor Cocktail 2 (Cat. No. P5726; Sigma Aldrich) and Cocktail 3 (Cat. No. P0044; Sigma Aldrich). Organoid lysates were sonicated using Sonics Vibra cell VCX130 (Sonics & Materials Inc., Newtown, USA) using a 50 % amplitude four times for 10 s. Protein concentration was measured using Pierce BCA Protein Assay Kit (ThermoScientific, Rockford, IL, USA). All samples were adjusted to the lowest protein concentration value. Lysates were then processed as previously described [74]. For liver samples, signals were normalized to a loading control (β-actin). For intestinal samples, most housekeeping proteins were downregulated upon amino acid depletion, therefore, signals were normalized to total amount of protein in the lane measured using SimplyBlue SafeStain (Thermo Fisher).

5.11. High resolution respirometry

Hepatic organoids were collected in Ad.DMEM/F12 at 4 °C and kept on ice for 10 min to properly disrupt the Matrigel. After centrifugation at 200*g* for 5 min at 4 °C, supernatant was removed and organoids were washed with MiR05 buffer followed by another centrifugation step. Organoids were then resuspended in 600 μl of MiR05 buffer (110 mM sucrose, 60 mM potassium lactobionate, 20 mM taurine, 20 mM HEPES, 0.5 mM EGTA, 10 mM KH2PO4, 3 mM MgCl2, 1 mg/ml bovine serum albumin, pH 7.1).

The rate of oxygen consumption of the organoids was measured using a two-channel high-resolution Oroboros Oxygraph-2 k (Oroboros, Innsbruck, Austria) at 37 °C. Firstly, organoids were provided with 1

mM ADP. Maximal ADP-stimulated respiration was achieved by addition of the oxidable substrates Palmitoyl Carnitine (25uM) plus Malate (2 mM) to stimulate the fatty acid β-oxidation (State 3). Next, basal respiration (state 4) was determined using Oligomycin to block ATP synthase. Finally, 0.5 mM FCCP was added in order to study the oxygen consumption during uncoupled respiration (State U). Oxygen consumption rates were normalized for protein content.

5.12. Mitochondrial copy number

Organoids were collected in basal AdvDMEM/F12 and lysed in lysis buffer (100 mM Tris-HCL pH 8.5, 5 mM EDTA, 0.2 % SDS, 200 mM NaCl and 20 mg/ml proteinase K) for 2 h prior to the addition of RNase A. Isopropanol was used to precipitate the DNA, and the pellet was washed with 70 % ethanol. After centrifugation at max. speed at 4 °C, the pellet was resuspended in TE buffer and DNA yields were measured. qPCR reactions were performed using FastStart Universal SYBR Green Master (Rox) (Sigma Aldrich) in 384 well format in duplicate with 10 ng (for the intestinal samples) and 20 ng (for the hepatic samples) total DNA per well in a QuantStudio 7 Flex. Mitochondrial DNA was measured using home-made primers (Supplementary Table 2) and normalized to the values of nuclear β-globulin as reference.

5.13. Branched chain fatty acid and very long chain fatty acid measurements

Mature hepatic organoids were incubated with 25 μM phytol (Sigma Aldrich) for 48 h prior to quenching in ice-cold methanol. Methanol was evaporated at 37 °C under a steady stream of N_2 for 40 min. Next, the pellet was reconstituted in PBS. Samples were hydrolysed in two steps. First, an acid hydrolysis step was performed to release the fatty acids from the different moieties they are bound to without affecting phytanic acid. This was followed by a basic hydrolysis to convert esterified fatty acids into free fatty acids. Pentafluorobenzyl bromide (PFB-Br) was added for the derivatization. The PFB derivatives were analysed on the GC/MS (Agilent 7890/5975 inert XL GCMS System, Agilent Technologies, Amstelveen, The Netherlands) in negative chemical ionization mode (NCI). Results were normalized for protein content.

5.14. Acylcarnitines measurements

Mature hepatic organoids were incubated with 1 mM L-carnitine (Sigma Aldrich) for 24 h prior to collection in TBS. Intracellular acylcarnitines were measured following the previously published protocol [73].

5.15. Imaging of the liver and intestinal organoids and processing of the images

Organoid cultures were followed over time with an AxioObserver Z1 compound microscope (Carl Zeiss), 2.5× and 5× objectives and an AxioCam MRm3 CCD camera (Carl Zeiss). Raw images were processed using the ZEN 3.1 blue edition software. The number and size of organoids were assessed in the whole well. A set of 25 organoids were manually counted in each well, tracked over time and measured throughout the different time points.

5.16. Statistical analysis

All results are expressed as mean ± standard error of the mean (SEM) as indicated. Biological replicates are considered as independent experiments. Group differences were assessed with repeated measures ANOVA for multiple day organoids size measurements or an ordinary one or two-way ANOVA with Tukey's post hoc multiple comparisons analyses. Statistical analysis was performed with GraphPad Prism Software Version 9.02 (Graphpad Software, San Diego, California USA). Statistical significance was given as $***P$ value < 0.001, $**P$ value < 0.01 and $*P$ value < 0.5; NS or no indication means no significant changes.

Funding

This work was supported by the European Union's Horizon 2020 research and innovation programme under the Marie Skłodowska-Curie grant agreement No 812968; the Canadian Institutes of Health Research (156307); and the Stichting De Cock-Hadders.

CRediT authorship contribution statement

José M. Horcas-Nieto: Conceptualization, Methodology, Validation, Formal analysis, Investigation, Resources, Writing – original draft, Writing – review & editing, Visualization. **Christian J. Versloot:** Conceptualization, Methodology, Validation, Formal analysis, Investigation, Resources, Writing – original draft, Writing – review & editing, Visualization. **Miriam Langelaar-Makkinje:** Methodology, Validation, Resources, Investigation. **Albert Gerding:** Methodology, Validation, Resources, Investigation. **Tjasso Blokzijl:** Resources. **Mirjam H. Koster:** Resources, Investigation. **Mirjam Baanstra:** Resources. **Ingrid A. Martini:** Investigation. **Robert P. Coppes:** Resources. **Céline Bourdon:** Formal analysis. **Sven C.D. van Ijzendoorn:** Resources. **Peter Kim:** Writing – review & editing, Supervision. **Robert H.J. Bandsma:** Conceptualization, Writing – original draft, Writing – review & editing, Supervision, Funding acquisition. **Barbara M. Bakker:** Conceptualization, Writing – original draft, Writing – review & editing, Supervision, Project administration, Funding acquisition.

Declaration of competing interest

The authors declare that they have no known competing financial interests or personal relationships that could have appeared to influence the work reported in this paper.

Data availability

Data will be made available on request.

Acknowledgements

We would like to thank Karen van Eunen, Niels Kloosterhuis and Marieke Smit for their technical support with intestinal organoids and animal work. We would also like to acknowledge Hans Clevers, Tomohiro Mizutani, Jeroen Korving and Klaas Nico Faber for their advice on culturing of organoids.

Appendix A. Supplementary data

Supplementary data to this article can be found online at https://doi.org/10.1016/j.bbadis.2022.166635.

References

[1] T. Sato, et al., Single Lgr5 stem cells build crypt-villus structures in vitro without a mesenchymal niche, Nature 459 (2009) 262–265.
[2] M. Huch, et al., In vitro expansion of single Lgr5+ liver stem cells induced by Wnt-driven regeneration, Nature 494 (2013) 247–250.
[3] M. Huch, B.-K. Koo, Modeling mouse and human development using organoid cultures, Development 142 (2015) 3113–3125.
[4] D. Dutta, I. Heo, H. Clevers, Disease modeling in stem cell-derived 3D organoid systems, Trends Mol. Med. 23 (2017) 393–410.
[5] H. Clevers, Modeling development and disease with organoids, Cell 165 (2016) 1586–1597.
[6] I.A. Okkelman, N. Neto, D.B. Papkovsky, M.G. Monaghan, R.I. Dmitriev, A deeper understanding of intestinal organoid metabolism revealed by combining fluorescence lifetime imaging microscopy (FLIM) and extracellular flux analyses, Redox Biol. 30 (2020), 101420.

[7] H.S. Kruitwagen, et al., Long-term adult feline liver organoid cultures for disease modeling of hepatic steatosis, Stem Cell Rep. 8 (2017) 822–830.
[8] T. Cai, et al., Effects of six common dietary nutrients on murine intestinal organoid growth, PLoS One 13 (2018), e0191517.
[9] Y. Chen, M. Michalak, L.B. Agellon, Importance of nutrients and nutrient metabolism on human health, Yale J. Biol. Med. 91 (2018) 95–103.
[10] André Briend, Kwashiorkor: still an enigma – the search must go on, 2014.
[11] S. Attia, et al., Mortality in children with complicated severe acute malnutrition is related to intestinal and systemic inflammation: an observational cohort study, Am. J. Clin. Nutr. 104 (2016) 1441–1449.
[12] M. Kerac, et al., Follow-up of post-discharge growth and mortality after treatment for severe acute malnutrition (FuSAM study): a prospective cohort study, PLoS One 9 (2014), e96030.
[13] T. Munthali, C. Jacobs, L. Sitali, R. Dambe, C. Michelo, Mortality and morbidity patterns in under-five children with severe acute malnutrition (SAM) in Zambia: a five-year retrospective review of hospital-based records (2009–2013), Arch. Public Health 73 (2015) 23.
[14] A.C. Ubesie, N.S. Ibeziako, C.I. Ndiokwelu, C.M. Uzoka, C.A. Nwafor, Under-five protein energy malnutrition admitted at the University of Nigeria Teaching Hospital, Enugu: a 10 year retrospective review, Nutr. J. 11 (2012) 43.
[15] B. Wharton, Hypoglycaemia in children with kwashiorkor, Lancet 1 (1970) 171–173.
[16] T. Nduhukire, D. Atwine, L. Rachel, J.E. Byonanebye, Predictors of in-hospital mortality among under-five children with severe acute malnutrition in South-Western Uganda, PLoS One 15 (2020), e0234343.
[17] R.H.J. Bandsma, et al., Mechanisms behind decreased endogenous glucose production in malnourished children, Pediatr. Res. 68 (2010) 423–428.
[18] B. Grenov, et al., Diarrhea, dehydration, and the associated mortality in children with complicated severe acute malnutrition: a prospective cohort study in Uganda, J. Pediatr. 210 (2019) 26–33.
[19] A.V. Badaloo, T. Forrester, M. Reid, F. Jahoor, Lipid kinetic differences between children with kwashiorkor and those with marasmus, Am. J. Clin. Nutr. 83 (2006) 1283–1288.
[20] A. Badaloo, M. Reid, D. Soares, T. Forrester, F. Jahoor, Relation between liver fat content and the rate of VLDL apolipoprotein B-100 synthesis in children with protein-energy malnutrition, Am. J. Clin. Nutr. 81 (2005) 1126–1132.
[21] S.E. Brooks, M.H. Goldon, E. Taylor, Hepatic ultrastructure in children with protein-energy malnutrition, West Indian Med. J. 41 (1992) 139–145.
[22] M. Shiner, A.O. Redmond, J.D. Hansen, The jejunal mucosa in protein-energy malnutrition. A clinical, histological, and ultrastructural study, Exp. Mol. Pathol. 19 (1973) 61–78.
[23] J.V. Campos, et al., Jejunal mucosa in marasmic children. Clinical, pathological, and fine structural evaluation of the effect of protein-energy malnutrition and environmental contamination, Am. J. Clin. Nutr. 32 (1979) 1575–1591.
[24] O. Brunser, C. Castillo, M. Araya, Fine structure of the small intestinal mucosa in infantile marasmic malnutrition, Gastroenterology 70 (1976) 495–507.
[25] J.J. Theron, W. Wittmann, J.G. Prinsloo, The fine structure of the jejunum in kwashiorkor, Exp. Mol. Pathol. 14 (1971) 184–199.
[26] E. Rath, A. Moschetta, D. Haller, Mitochondrial function - gatekeeper of intestinal epithelial cell homeostasis, Nat. Rev. Gastroenterol. Hepatol. 15 (2018) 497–516.
[27] M.C. Ludikhuize, et al., Mitochondria define intestinal stem cell differentiation downstream of a FOXO/Notch axis, Cell Metab. 32 (2020) 889–900.e7.
[28] F. Lopes, et al., ER-stress mobilization of death-associated protein kinase-1-dependent xenophagy counteracts mitochondria stress-induced epithelial barrier dysfunction, J. Biol. Chem. 293 (2018) 3073–3087.
[29] G. Sargent, et al., PEX2 is the E3 ubiquitin ligase required for pexophagy during starvation, J. Cell Biol. 214 (2016) 677–690.
[30] T. van Zutphen, et al., Malnutrition-associated liver steatosis and ATP depletion is caused by peroxisomal and mitochondrial dysfunction, J. Hepatol. 65 (2016) 1198–1208.
[31] M.A. Johnson, et al., Amino acid starvation has opposite effects on mitochondrial and cytosolic protein synthesis, PLoS One 9 (2014), e93597.
[32] G. Fabris, O. Dumortier, D.F. Pisani, N. Gautier, E. Van Obberghen, Amino acid-induced regulation of hepatocyte growth: possible role of drosha, Cell Death Dis. 10 (2019) 566.
[33] H. Hu, et al., Long-term expansion of functional mouse and human hepatocytes as 3D organoids, Cell 175 (2018) 1591–1606.e19.
[34] N.C. Zachos, et al., Human enteroids/colonoids and intestinal organoids functionally recapitulate Normal intestinal physiology and pathophysiology, J. Biol. Chem. 291 (2016) 3759–3766.
[35] L. Broutier, et al., Culture and establishment of self-renewing human and mouse adult liver and pancreas 3D organoids and their genetic manipulation, Nat. Protoc. 11 (2016) 1724–1743.
[36] E.M. Brown, et al., Diet and specific microbial exposure trigger features of environmental enteropathy in a novel murine model, Nat. Commun. 6 (2015) 7806.
[37] T.-Y. Huang, et al., Overexpression of PGC-1α increases peroxisomal activity and mitochondrial fatty acid oxidation in human primary myotubes, Am. J. Physiol. Endocrinol. Metab. 312 (2017) E253–E263.
[38] T. Imanaka, K. Aihara, Y. Suzuki, S. Yokota, T. Osumi, The 70-kDa peroxisomal membrane protein (PMP70), an ATP-binding cassette transporter, Cell Biochem. Biophys. 32 (2000) 131–138.
[39] R.J.A. Wanders, J. Komen, S. Ferdinandusse, Phytanic acid metabolism in health and disease, Biochim. Biophys. Acta 1811 (2011) 498–507.
[40] N.E. Braverman, M.D. D'Agostino, G.E. MacLean, Peroxisome biogenesis disorders: biological, clinical and pathophysiological perspectives, Dev. Disabil. Res. Rev. 17 (2013) 187–196.
[41] G. Du, et al., Peroxisome elevation induces stem cell differentiation and intestinal epithelial repair, Dev. Cell 53 (2020) 169–184.e11.
[42] Y. Wada, Y. Takeda, M. Kuwahata, Potential role of amino acid/protein nutrition and exercise in serum albumin redox state, Nutrients 10 (2017).
[43] J.F. Morlese, et al., Albumin kinetics in edematous and nonedematous protein-energy malnourished children, Am. J. Clin. Nutr. 64 (1996) 952–959.
[44] C.D. Williams, A nutritional disease of childhood associated with a maize diet, Arch. Dis. Child. 8 (1933) 423–433.
[45] G. Hu, et al., The role of tryptophan-nicotinamide (TRP-NAM) pathway in malnutrition induced liver dysfunction, Curr. Dev. Nutr. 4 (Suppl 2) (2020 May 29) 688, https://doi.org/10.1093/cdn/nzaa050_011.
[46] S. Cassim, V.-A. Raymond, P. Lapierre, M. Bilodeau, From in vivo to in vitro: major metabolic alterations take place in hepatocytes during and following isolation, PLoS One 12 (2017), e0190366.
[47] S.R. Nagarajan, et al., Lipid and glucose metabolism in hepatocyte cell lines and primary mouse hepatocytes: a comprehensive resource for in vitro studies of hepatic metabolism, Am. J. Physiol. Endocrinol. Metab. 316 (2019) E578–E589.
[48] W.C. Peng, et al., Inflammatory cytokine TNFα promotes the long-term expansion of primary hepatocytes in 3D culture, Cell 175 (2018) 1607–1619.e15.
[49] S.R. Moore, et al., Glutamine and alanyl-glutamine promote crypt expansion and mTOR signaling in murine enteroids, Am. J. Physiol. Gastrointest. Liver Physiol. 308 (2015) G831–G839.
[50] Y. Saito, et al., Effect of essential amino acids on enteroids: methionine deprivation suppresses proliferation and affects differentiation in enteroid stem cells, Biochem. Biophys. Res. Commun. 488 (2017) 171–176.
[51] C.A. Richmond, M.S. Shah, D.L. Carlone, D.T. Breault, An enduring role for quiescent stem cells, Dev. Dyn. 245 (2016) 718–726.
[52] S.J.A. Buczacki, et al., Intestinal label-retaining cells are secretory precursors expressing Lgr5, Nature 495 (2013) 65–69.
[53] J.H. van Es, et al., Dll1+ secretory progenitor cells revert to stem cells upon crypt damage, Nat. Cell Biol. 14 (2012) 1099–1104.
[54] P.W. Tetteh, et al., Replacement of lost Lgr5-positive stem cells through plasticity of their enterocyte-lineage daughters, Cell Stem Cell 18 (2016) 203–213.
[55] U. Jadhav, et al., Dynamic reorganization of chromatin accessibility signatures during dedifferentiation of secretory precursors into Lgr5+ intestinal stem cells, Cell Stem Cell 21 (2017) 65–77.e5.
[56] B. Amadi, et al., Impaired barrier function and autoantibody generation in malnutrition enteropathy in Zambia, EBioMedicine 22 (2017) 191–199.
[57] M. Farràs, et al., Characterizing the metabolic phenotype of intestinal villus blunting in Zambian children with severe acute malnutrition and persistent diarrhea, PLoS One 13 (2018), e0192092.
[58] R.T. Boaz, A.J. Joseph, G. Kang, A. Bose, Intestinal permeability in normally nourished and malnourished children with and without diarrhea, Indian Pediatr. 50 (2013) 152–153.
[59] S. Khaloian, et al., Mitochondrial impairment drives intestinal stem cell transition into dysfunctional Paneth cells predicting Crohn's disease recurrence, Gut 69 (2020) 1939–1951.
[60] S. Hara-Kuge, Y. Fujiki, The peroxin Pex14p is involved in LC3-dependent degradation of mammalian peroxisomes, Exp. Cell Res. 314 (2008) 3531–3541.
[61] L. Jiang, S. Hara-Kuge, S.-I. Yamashita, Y. Fujiki, Peroxin Pex14p is the key component for coordinated autophagic degradation of mammalian peroxisomes by direct binding to LC3-II, Genes Cells 20 (2015) 36–49.
[62] A. Peeters, et al., Mitochondria in peroxisome-deficient hepatocytes exhibit impaired respiration, depleted DNA, and PGC-1α independent proliferation, Biochim. Biophys. Acta 1853 (2015) 285–298.
[63] F. Roels, et al., Different types of peroxisomes in human duodenal epithelium, Gut 32 (1991) 858–865.
[64] F. Di Cara, M.H. Bülow, A.J. Simmonds, R.A. Rachubinski, Dysfunctional peroxisomes compromise gut structure and host defense by increased cell death and Tor-dependent autophagy, Mol. Biol. Cell 29 (2018) 2766–2783.
[65] F. Yan, et al., Peroxisome proliferator-activated receptor α activation induces hepatic steatosis, suggesting an adverse effect, PLoS One 9 (2014).
[66] M. Kiskac, et al., A case of rhabdomyolysis complicated with acute renal failure after resumption of fenofibrate therapy: a first report, Indian J. Pharmacol. 45 (2013) 305–306.
[67] D. Rigano, C. Sirignano, O. Taglialatela-Scafati, The potential of natural products for targeting PPARα, Acta Pharm. Sin. B 7 (2017) 427–438.
[68] H. Keller, et al., Fatty acids and retinoids control lipid metabolism through activation of peroxisome proliferator-activated receptor-retinoid X receptor heterodimers, Proc. Natl. Acad. Sci. U. S. A. 90 (1993) 2160–2164.
[69] A. Bartolomé, et al., MTORC1 regulates both general autophagy and mitophagy induction after oxidative phosphorylation uncoupling, Mol. Cell. Biol. 37 (2017).
[70] N. Pentinmikko, et al., Notum produced by Paneth cells attenuates regeneration of aged intestinal epithelium, Nature 571 (2019) 398–402.
[71] S. Gidfar, et al., Rapamycin prolongs the survival of corneal epithelial cells in culture, Sci. Rep. 7 (2017).
[72] J. Sunayama, et al., Dual blocking of mTor and PI3K elicits a prodifferentiation effect on glioblastoma stem-like cells, Neuro-Oncology 12 (2010) 1205–1219.
[73] B. Evers, et al., Simultaneous quantification of the concentration and carbon isotopologue distribution of polar metabolites in a single analysis by gas chromatography and mass spectrometry, Anal. Chem. 93 (2021) 8248–8256.
[74] A.M. Heberle, et al., The PI3K and MAPK/p38 pathways control stress granule assembly in a hierarchical manner, Life Sci. Alliance 2 (2019).